Comparison of Finite-Element Based State-Space Models for PM Synchronous Machines

Paavo Rasilo, Marc-Antoine Lemesle, Anouar Belahcen, Antero Arkkio, and Marko Hinkkanen

***Abstract*—An interior-permanent-magnet motor is modeled by a combined analytical-numerical approach, in which the relationships between the stator currents and flux linkages are identified with static finite-element (FE) analysis. In addition to the previous approaches using the current space vector as the state variable, new models are also developed using the flux-linkage space vector, which leads to more convenient time-integration of the voltage equations. In order to account for the zero-sequence effects in delta connection, the models also include either the zero-sequence flux or current as an additional state variable. Finally, the possibilities of deriving the required quantities as partial derivatives of the magnetic field energy are discussed. The energy-based approaches avoid inaccuracies related to torque computation and thus allow better satisfying the power balance in the state-space model. We show the ability of the developed state-space models to predict the currents and torque equally to a nonlinear time-stepping FE model with much less computational burden. The results are validated by means of measurements for a prototype machine in both star and delta connections. In addition, we also demonstrate the effect of the zero-sequence current on the torque ripple in case of a delta-connected stator winding.**

***Index Terms*—Field energy, finite element methods, magnetic saturation, permanent magnet machines, reluctance machines, state-space methods, torque ripple, variable speed drives.**

I. Introduction

PERMANENT-MAGNET (PM) synchronous machines with interior magnets have become popular in variable-speed applications as both motors and generators. Their main advantages are high power densities, relatively simple construction, small rotor losses as well as the possibility of taking advantage of the reluctance torque owing to the magnetic saliency [1]. However, the spatial permeance harmonics due to the saliency and the interaction of the permanent magnet flux with the stator slotting also cause unwanted ripple in the electromagnetic torque of the machine [2]. The torque ripple typically deteriorates the properties of the application and may excite mechanical resonances. In addition, the harmonic effects complicate the modeling of the machine.

Manuscript submitted December 12, 2013. The authors thank ABB Oy and the Academy of Finland for financial support.

P. Rasilo, A. Belahcen, A. Arkkio, and M. Hinkkanen are with the Aalto University School of Electrical Engineering, Department of Electrical Engineering, P.O. Box 13000, FI-00076 Aalto, Finland. P. Rasilo is also with the Ghent University, Sint-Pietersnieuwstraat 41, B-9000, Ghent, Belgium. M.-A. Lemesle is with Polytech Nantes, BP 152, F-44603 St-Nazaire Cedex, France. E-mail: paavo.rasilo@alumni.aalto.fi.

The voltage equations for a PM synchronous machine can be written as

$$\boldsymbol{u} = R_\mathrm{s}\boldsymbol{i} + \frac{d\boldsymbol{\psi}}{dt}, \tag{1}$$

in which the column vectors $\boldsymbol{u}$, $\boldsymbol{i}$ and $\boldsymbol{\psi}$ include either the phase-domain or two-axis components (in the stator frame of reference) of the voltage, current and flux linkage, respectively, and R_s is the resistance of a stator phase. When solving this system, the relationship between the current and flux linkage is usually expressed using analytical inductance functions, the simplest ones of which reduce to constant inductances when (1) is transformed into the rotor direct-quadrature (d-q) frame of reference. This traditional d-q model only accounts for the fundamental spatial permeance variation and neglects magnetic saturation. Although more complicated functions for both higher-order permeance harmonics [3]-[6] and saturation [7]-[9] have been proposed, the problem is in general too dependent on the machine geometry and material properties to justify the validity of the analytical models if very accurate models are desired. Especially, design tools for control and estimation algorithms require accurate prediction of the nonidealities of the machines.

Finite-element (FE) method (FEM) based models provide an alternative for the analytical approaches. While time-stepping FE models, such as [10] and [11], are able to more accurately account for the time harmonics, actual geometry, and the nonlinear material properties, they are generally too slow to be used for control design problems, which typically require simulation of tens or hundreds of supply periods. However, precalculated static FE results can be used in the state-space models to replace the analytical inductance functions. Such approaches have been starting to gain increasing attention during the recent years, although from quite a limited number of research groups so far [12]-[21]. Below, these approaches are briefly reviewed and discussed.

In [12] and [13], phase-domain models were developed both for a healthy PM motor and for one with an inter-turn short circuit in one of the phase windings. The model was identified by obtaining the winding inductances, permanent-magnet flux and cogging torque from transient 2-D FE simulations. In [14], the approach was used for inductance calculation in a sensorless control application with an electromotive-force observer. The models of [12] and [13] neglected saturation based on the assumption that the total flux linkage of the windings is dominated by the PM flux. The same was assumed in [15] and [16] which used 2-D FEM to identify the linear inductances for both phase-domain and two-axis models of a

double-star interior-magnet machine. All the circuit models of [12], [13], [15], and [16] were implemented in the MATLAB/Simulink environment using look-up tables (LUT). In [17] and [18], saturation was also included in both phase-domain and two-axis PM machine models which were implemented on a real-time FPGA simulator.

Instead of calculating the inductance functions using FEM, [19]-[21] directly identified the flux linkages of the windings as functions of the currents and the rotor angle. This would not be beneficial in the linear cases of [12], [13], [15], and [16] in which one inductance function describes the behavior for the whole range of currents. In general, however, it is easier to obtain the flux linkages than the inductances from the FE solution. Indeed, numerical inductance calculations require supplying current into one winding at the time, and still calculating the flux linkages of all the windings separately. In addition, the nonlinear case requires freezing the permeabilities of iron into the desired operation point, as also stated in [19].

A common feature for all the reviewed methods [12]-[21] is that they all use the currents as the state variables together with the (electrical) rotor angle α_r. With this approach, (1) becomes

$$\boldsymbol{u} = R_s \boldsymbol{i} + \frac{\partial \boldsymbol{\psi}(\boldsymbol{i}, \alpha_r)}{\partial \boldsymbol{i}} \frac{d\boldsymbol{i}}{dt} + \omega_r \frac{\partial \boldsymbol{\psi}(\boldsymbol{i}, \alpha_r)}{\partial \alpha_r}, \tag{2}$$

in which $\omega_r = d\alpha_r / dt$ is the rotation speed. The disadvantage of the current-based model (2) is that it requires calculating and inverting the differential inductance matrix $\partial \boldsymbol{\psi} / \partial \boldsymbol{i}$ during the solution. On the contrary, choosing the flux linkage as the state variable results in

$$\boldsymbol{u} = R_s \boldsymbol{i}(\boldsymbol{\psi}, \alpha_r) + \frac{d\boldsymbol{\psi}}{dt}, \tag{3}$$

and thus removes the need for calculating or storing the partial derivatives yielding a simpler and faster solution. However, if skewing or other axial effects are to be modeled, the current-based approach allows coupling multiple axial slices in the state-space model while employing data only from a single 2-D FE model [21]. This is a significant advantage of the current-based models, since the slice model does not have to be implemented in FEM. The same is much more difficult with the flux-based model since continuity of the currents between the slices has to be ensured.

Another important part of modeling the PM machines is the calculation of the electromagnetic torque. Several different approaches were applied in the reviewed papers. In [12], [13], and [15], the torque was obtained by calculating the flux-current contribution assuming a linear material and summing to this the cogging torque determined by FE analysis, while [16] completely neglected the cogging torque. In a general nonlinear case, however, the torque should be obtained by the virtual work principle as a partial derivative of the magnetic field energy W_f or co-energy W_c with respect to the mechanical rotor angle, keeping the other variables constant:

$$T = -p \frac{\partial W_f(\boldsymbol{\psi}, \alpha_r)}{\partial \alpha_r} = p \frac{\partial W_c(\boldsymbol{i}, \alpha_r)}{\partial \alpha_r}, \tag{4}$$

in which p is the number of pole pairs [22]. Another way is to directly interpolate the torque from precalculated FE results, as was done in [17]-[21].

Finally, [12]-[21] only focused on star-connected machines thus assuming that no zero-sequence current flows in the stator windings. Although plain delta connection is quite rarely used in variable-speed PM machines, recent attention has been given to multiple-step star-delta connected windings [23], [24] which can be used, e.g., for terminal voltage adjustment in variable-speed generators. For analysis of machines with such winding configurations, the zero-sequence current also needs to be considered.

In this paper, we develop and compare FE-based state-space models for a 2.2-kW PM machine with the possibility of taking into account the effects of the zero-sequence current. Three different state-variable choices are studied. In current- and flux-based models (CBM and FBM, respectively), the space vectors and zero-sequence components of the stator current and flux linkage are used. In addition, a hybrid model (HM) is studied in which the flux-linkage space vector and the zero-sequence current are chosen as the state variables. In the case of the CBM, a slice model is implemented in order to model the skewed rotor of the test machine. In case of the FBM, we also study an energy-based model (FBME) in which the currents and electromagnetic torque are derived from the FE-calculated magnetic field energy instead of merely interpolating from the results stored in LUTs. The aim is to avoid errors in the torque calculation from the FE solution and thus better satisfy the power balance in the state-space model.

The results of the developed state-space models are shown to correspond well to both time-stepping FE analysis and measurement results both in star and delta connections. Using both the time-stepping FE method and the developed state-space model, we demonstrate the significant effect of the zero-sequence current on the torque ripple of the machine. This effect is visible in the results of [23] and [24] but has not been properly discussed earlier.

II. Studied Machine and Measurement Setup

The machine used both in the simulations and for the experimental studies is a 2.2-kW, 370-V, 75-Hz, 6-pole interior-magnet PM machine. The FE mesh and some data and dimensions of the machine are given in Fig. 1 and Table I, respectively. The rotor of the machine consists of two axial modules of the same length, which have been phase shifted from each other by 5° (mechanical) to reduce the cogging torque.

The machine is a prototype having a construction of a mass-produced industrial motor which are applicable with both 690-V and 400-V supplies. The machine thus has a full-pitched stator winding which can be connected either in star or delta, as desired. This offers an excellent possibility to study the zero-sequence effects and thus allows validation of the developed models in both star and delta connections.

The phase currents of the machine were measured by current shunts to allow calculation of the zero-sequence current. By phase quantities (denoted by subscripts abc) we refer to the currents, voltages and flux linkages of the actual windings inside the machine, not the terminal quantities seen from the

outside of the machine. The meaning of the phase quantities is thus independent of the connection of the windings. For clarity, Fig. 2 presents the phase and terminal quantities for both star and delta connections.

To determine the operation point of the machine, the rotation speed was calculated directly from the supply frequency and the torque was obtained with a double-bearing arrangement and a piezoelectric force measurement. In addition, the root-mean-squared (rms) terminal currents and voltages as well as the terminal powers were recorded with a LEM Norma 6000 D power analyzer.

III. Methods of Modeling

A. State-Space Models and Choice of State Variables

We focus on solving (1) in the two-axis form and stator (x-y) frame of reference. In addition to the two-axis quantities, also the zero-sequence current and flux are considered. The zero-sequence (subscript 0) is defined as the average value of the phase quantities, e.g. for the flux linkage,

$$\psi_0 = \frac{\psi_a + \psi_b + \psi_c}{3}. \quad (5)$$

In a three-phase machine, the zero-sequence flux linkage arises from the spatial air-gap flux-density harmonics having an order of multiple of three, which impose equal flux linkages through each phase winding simultaneously. These harmonics arise from magnetic saturation as well as the interaction of the even permeance harmonics with the odd magnetomotive force harmonics. The possibility for the existence of the zero-sequence current is defined by the winding connection. In the delta connection, the zero-sequence current can flow freely, contrary to the star connection with a floating star point, in which the zero-sequence current does not have a return path.

When the machine is supplied by the line-to-line voltages, the zero-sequence voltage is defined by the zero-sequence flux in the star connection, and is zero in the delta connection. Thus the zero-sequence voltage equation can be written as

$$u_0 = R_{s0} i_0 + \frac{d\psi_0}{dt}, \quad (6)$$

in which the resistance R_{s0} depends on the connection of the stator winding. In the star connection with a floating star point, the circuit is open (i.e. $R_{s0} = \infty$ which leads to $i_0 = 0$) and (6) can be neglected, while for the delta connection, $R_{s0} = R_s$ and $u_0 = 0$.

Due to the nonlinear dependency of the flux linkages and currents on each other and the rotor angle, we avoid using analytical inductance functions and express the relationships between the currents $\boldsymbol{i}_{xy0}$ and the flux linkages $\boldsymbol{\psi}_{xy0}$ using results of 2-D static FE analysis. However, there are different possibilities to choose the state variables for the model. Below, the advantages of different choices are briefly discussed. The main differences between the cases lie in the amount of numerical data needed to be stored in lookup tables (LUT) for the state-space model, the possibilities of modeling both star and delta connections using the same FE data, as well as the difficulties in derivation of the quantities from the magnetic field energy.

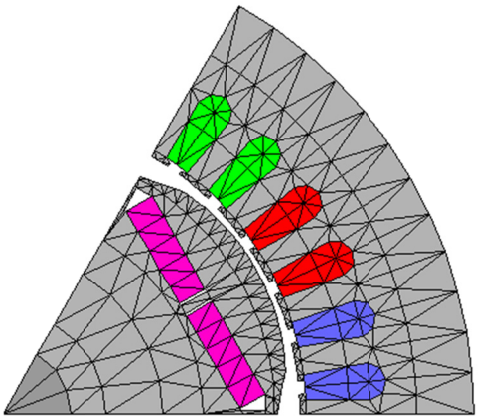

Fig. 1 FE mesh of the studied machine.

TABLE I
DATA AND DIMENSIONS OF THE TEST MACHINE

Machine type	motor
Power	2.2 kW
Voltage	370 V
Current	4.14 A
Displacement factor	0.926
Frequency	75 Hz
Connection	delta
Number of pole pairs	3
Stator outer diameter	165 mm
Stator inner diameter	104 mm
Air gap	1 mm
Number of stator slots	36

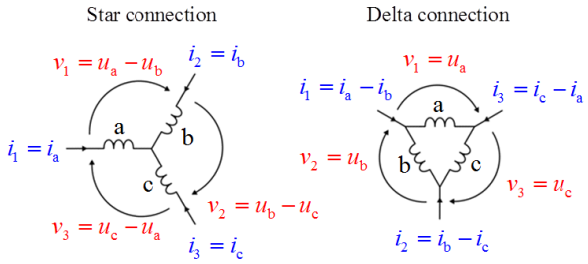

Fig. 2 Notation for the phase (abc) and terminal (123) voltages and currents in star and delta connections.

1) Current-based model (CBM)

The currents were used as the state variables in all the models of [12]-[21]. In the considered xy0-system, the state variables of the current-based model are $\boldsymbol{i}_{xy}$, i_0 and the rotor angle α_r. The advantage of choosing the currents as the state variables is that the current supply is easy to implement in the static FE analysis and that both star and delta connections can be modeled, since the zero-sequence current can be forced to zero in the former. The resulting state-space form of (1) becomes

$$\frac{d\boldsymbol{i}_{xy(0)}}{dt} = \left(\frac{\partial \boldsymbol{\psi}_{xy(0)}}{\partial \boldsymbol{i}_{xy(0)}}\right)^{-1} \left(\boldsymbol{u}_{xy(0)} - R_s \boldsymbol{i}_{xy(0)} - \omega_r \frac{\partial \boldsymbol{\psi}_{xy(0)}}{\partial \alpha_r}\right), \quad (7)$$

in which the notation xy(0) means that the zero-sequence voltage equation can be neglected for the star connection. This makes the star-connected case only a special case of (7), in which the zero-sequence current is not included. The model requires storing the stator flux-linkage vectors calculated with FE analysis as

$$\boldsymbol{\psi}_{\mathrm{xy(0)}} = \boldsymbol{\psi}_{\mathrm{xy(0),FE}}\left(\boldsymbol{i}_{\mathrm{xy(0)}}, \alpha_{\mathrm{r}}\right). \tag{8}$$

We implemented the current-based approach in the MATLAB/Simulink environment by deriving the three or six elements (assuming symmetry) of the Jacobian matrix $\partial\boldsymbol{\psi}_{\mathrm{xy(0)}} / \partial\boldsymbol{i}_{\mathrm{xy(0)}}$, the vector $\partial\boldsymbol{\psi}_{\mathrm{xy(0)}} / \partial\alpha_{\mathrm{r}}$, and the torque from the FE results and storing them in LUTs with linear interpolation. Since the rotor of our test machine is skewed, we also implemented the CBM by considering two axial slices and averaging the flux and torque over the slices as

$$\boldsymbol{\psi}_{\mathrm{xy(0)}} = \frac{\boldsymbol{\psi}_{\mathrm{xy(0),FE}}\left(\boldsymbol{i}_{\mathrm{xy(0)}}, \alpha_{\mathrm{r}}\right) + \boldsymbol{\psi}_{\mathrm{xy(0),FE}}\left(\boldsymbol{i}_{\mathrm{xy(0)}}, \alpha_{\mathrm{r}} + 15^{\circ}\right)}{2} \tag{9}$$

where 15° is the skew angle in electrical degrees.

2) Flux-based model (FBM)

In this approach, $\boldsymbol{\psi}_{\mathrm{xy}}$, ψ_0 and α_{r} are chosen as the state variables. This allows solving the voltage equations as

$$\frac{d\boldsymbol{\psi}_{\mathrm{xy(0)}}}{dt} = \boldsymbol{u}_{\mathrm{xy(0)}} - R_{\mathrm{s}}\boldsymbol{i}_{\mathrm{xy(0)}}, \tag{10}$$

and requires storing only the FE-calculated currents as functions of the state variables as

$$\boldsymbol{i}_{\mathrm{xy(0)}} = \boldsymbol{i}_{\mathrm{xy(0),FE}}\left(\boldsymbol{\psi}_{\mathrm{xy(0)}}, \alpha_{\mathrm{r}}\right), \tag{11}$$

which makes only two or three LUTs for the current plus one for the torque.

The model without the zero-sequence current might again seem to be only a special case of (10), in which the zero-sequence state and the corresponding equation are neglected. However, the FE results $\boldsymbol{i}_{\mathrm{xy0,FE}}(\boldsymbol{\psi}_{\mathrm{xy0}}, \alpha_{\mathrm{r}})$ required for the simulation of the delta-connected machine are not applicable for the simulation of the star-connected machine. This is due to the fact that the zero-sequence state variable is the flux linkage ψ_0 which is nonzero also in the star connection. In order to use the same data and still force the zero-sequence current to zero in the star connection, we would need to iteratively solve $i_{0,\mathrm{FE}}(\boldsymbol{\psi}_{\mathrm{xy0}}, \alpha_{\mathrm{r}}) = 0$ to find the correct value for ψ_0, which would be very time consuming. Consequently, to simulate the star-connected machine, a new set of FE simulations with three variables had to be made in order to obtain $\boldsymbol{i}_{\mathrm{xy,FE}}(\boldsymbol{\psi}_{\mathrm{xy}}, \alpha_{\mathrm{r}})$. In addition, another state-space model with only three state variables then had to be implemented.

In order to overcome the aforementioned disadvantage, and allow using a single model and the same FE data for both machine connections, we also study a case, in which the zero-sequence current is used as the fourth state variable together with the two-axis flux linkage and the rotor angle. Due to the use of both flux linkage and the current as the state variables, we refer to the approach as the *hybrid model*.

3) Hybrid model (HM)

This approach tries to combine the advantages of the CBM and FBM by choosing $\boldsymbol{\psi}_{\mathrm{xy}}$, i_0 and α_{r} as the state variables. Now, calculation of the Jacobian matrix $\partial\boldsymbol{\psi}_{\mathrm{xy}} / \partial\boldsymbol{i}_{\mathrm{xy}}$ is not needed since the two-axis fluxes are known. On the other hand, the star connection can also be modeled by forcing the zero-sequence current to zero. With this approach, the two-axis currents are known from the FE results as

$$\boldsymbol{i}_{\mathrm{xy}} = \boldsymbol{i}_{\mathrm{xy,FE}}\left(\boldsymbol{\psi}_{\mathrm{xy}}, i_0, \alpha_{\mathrm{r}}\right), \tag{12}$$

and the state-space form of (1) thus becomes

$$\frac{d\boldsymbol{\psi}_{\mathrm{xy}}}{dt} = \boldsymbol{u}_{\mathrm{xy}} - R_{\mathrm{s}}\boldsymbol{i}_{\mathrm{xy,FE}}\left(\boldsymbol{\psi}_{\mathrm{xy}}, i_0, \alpha_{\mathrm{r}}\right). \tag{13}$$

In a similar manner, the zero-sequence flux linkage can be expressed as

$$\psi_0 = \psi_{0,\mathrm{FE}}\left(\boldsymbol{\psi}_{\mathrm{xy}}, i_0, \alpha_{\mathrm{r}}\right), \tag{14}$$

after which the time-derivative in (6) becomes

$$\begin{aligned}\frac{d\psi_0}{dt} = {} & \frac{\partial\psi_{0,\mathrm{FE}}\left(\boldsymbol{\psi}_{\mathrm{xy}}, i_0, \alpha_{\mathrm{r}}\right)}{\partial\boldsymbol{\psi}_{\mathrm{xy}}}\frac{d\boldsymbol{\psi}_{\mathrm{xy}}}{dt} + \cdots \\ & + \frac{\partial\psi_{0,\mathrm{FE}}\left(\boldsymbol{\psi}_{\mathrm{xy}}, i_0, \alpha_{\mathrm{r}}\right)}{\partial i_0}\frac{di_0}{dt} + \cdots \\ & + \frac{\partial\psi_{0,\mathrm{FE}}\left(\boldsymbol{\psi}_{\mathrm{xy}}, i_0, \alpha_{\mathrm{r}}\right)}{\partial\alpha_{\mathrm{r}}}\frac{d\alpha_{\mathrm{r}}}{dt}.\end{aligned} \tag{15}$$

After substituting $\omega_{\mathrm{r}} = d\alpha_{\mathrm{r}} / dt$ and $d\boldsymbol{\psi}_{\mathrm{xy}} / dt$ from (13), the state-space form for i_0 in delta connection becomes

$$\frac{di_0}{dt} = -\frac{R_{\mathrm{s}}i_0 + \frac{\partial\psi_{0,\mathrm{FE}}}{\partial\boldsymbol{\psi}_{\mathrm{xy}}}\left(\boldsymbol{u}_{\mathrm{xy}} - R_{\mathrm{s}}\boldsymbol{i}_{\mathrm{xy}}\right) + \frac{\partial\psi_{0,\mathrm{FE}}}{\partial\alpha_{\mathrm{r}}}\omega_{\mathrm{r}}}{\partial\psi_{0,\mathrm{FE}} / \partial i_0}, \tag{16}$$

which together with (13) gives the complete state-space equations for this model.

This approach was implemented by storing $\boldsymbol{i}_{\mathrm{xy,FE}}$, the four partial derivatives in (16) and the torque in LUTs with linear interpolation. If the machine is star connected, $i_0 = 0$ and the solution of (16) can be neglected, which corresponds to the FBM for the star-connected machine.

4) Flux-based model with field energy (FBME)

Although the torque, two-axis currents, the zero-sequence current or flux linkage as well as the required partial derivatives can be obtained from FE analysis and stored in separate LUTs, they can also be derived starting from the magnetic field energy and co-energy. In principle a field-energy based model would allow avoiding any errors related to the computation of the electromagnetic torque from the FE solution [25] and thus possibly satisfy better the power balance during the simulations.

We derive the quantities from the field energy when using the FBM. When a differential change is imposed into the phase-domain flux linkages, the corresponding change in the

field energy is

$$dW_{\mathrm{f}} = i_{\mathrm{a}} d\psi_{\mathrm{a}} + i_{\mathrm{b}} d\psi_{\mathrm{b}} + i_{\mathrm{c}} d\psi_{\mathrm{c}} = \boldsymbol{i}_{\mathrm{abc}}^{\mathrm{T}} d\boldsymbol{\psi}_{\mathrm{abc}} . \quad (17)$$

If the phase quantities are expressed by multiplying the xy0-components by the inverse of the Park transformation matrix

$$\boldsymbol{T}_{\mathrm{xy0}} = \frac{1}{3}\begin{bmatrix} 2 & -1 & -1 \\ 0 & \sqrt{3} & -\sqrt{3} \\ 1 & 1 & 1 \end{bmatrix}, \quad (18)$$

we get

$$dW_{\mathrm{f}} = \boldsymbol{i}_{\mathrm{xy0}}^{\mathrm{T}} \left(\boldsymbol{T}_{\mathrm{xy0}}^{-1}\right)^{\mathrm{T}} \boldsymbol{T}_{\mathrm{xy0}}^{-1} d\boldsymbol{\psi}_{\mathrm{xy0}} = \frac{3}{2}\begin{bmatrix} 1 & 0 & 0 \\ 0 & 1 & 0 \\ 0 & 0 & 2 \end{bmatrix} \boldsymbol{i}_{\mathrm{xy0}}^{\mathrm{T}} d\boldsymbol{\psi}_{\mathrm{xy0}} . \quad (19)$$

Thus the xy0-components of the currents are obtained from the partial derivatives of the field energy as

$$\boldsymbol{i}_{\mathrm{xy0}} = \frac{1}{3}\begin{bmatrix} 2 & 0 & 0 \\ 0 & 2 & 0 \\ 0 & 0 & 1 \end{bmatrix} \left(\frac{\partial W_{\mathrm{f}}\left(\boldsymbol{\psi}_{\mathrm{xy0}}, \alpha_{\mathrm{r}}\right)}{\partial \boldsymbol{\psi}_{\mathrm{xy0}}} \right)^{\mathrm{T}} . \quad (20)$$

The electromagnetic torque is obtained from (4). Thus only the magnetic field energy $W_{\mathrm{f,FE}}$ is needed as the result of the FE analysis. A cubic-spline approximation is used for the field energy to make it differentiable.

B. Finite-Element Model

The FE model used for the identification of the torque and flux-current relations solves Ampere's circuital law in the 2-D cross section of the machine using the magnetic vector-potential formulation [11]. Nonlinear single-valued material properties are used for the iron, and the iron losses are neglected. Although static FE solvers are usually supplied by constant currents, the flux linkages can straightforwardly be enforced by adding extra equations for the xy0 components of the currents. In addition, the zero-sequence current can be easily imposed in the windings. The total FE systems for the identification of the CBM, FBM and HM, respectively, are

$$\boldsymbol{S}\left(\boldsymbol{a}, \alpha_{\mathrm{r}}\right)\boldsymbol{a} = \boldsymbol{f}_{\mathrm{pm}} + \boldsymbol{D}_{\mathrm{x}}^{\mathrm{T}} \boldsymbol{i}_{\mathrm{x}} + \boldsymbol{D}_{\mathrm{y}}^{\mathrm{T}} \boldsymbol{i}_{\mathrm{y}} + \boldsymbol{D}_{0}^{\mathrm{T}} \boldsymbol{i}_{0} , \quad (21)$$

$$\begin{bmatrix} \boldsymbol{S}\left(\boldsymbol{a}, \alpha_{\mathrm{r}}\right) & -\boldsymbol{D}_{\mathrm{x}}^{\mathrm{T}} & -\boldsymbol{D}_{\mathrm{y}}^{\mathrm{T}} & -\boldsymbol{D}_{0}^{\mathrm{T}} \\ l\boldsymbol{D}_{\mathrm{x}} & 0 & 0 & 0 \\ l\boldsymbol{D}_{\mathrm{y}} & 0 & 0 & 0 \\ l\boldsymbol{D}_{0} & 0 & 0 & 0 \end{bmatrix} \begin{bmatrix} \boldsymbol{a} \\ i_{\mathrm{x}} \\ i_{\mathrm{y}} \\ i_{0} \end{bmatrix} = \begin{bmatrix} \boldsymbol{f}_{\mathrm{pm}} \\ \psi_{\mathrm{x}} \\ \psi_{\mathrm{y}} \\ \psi_{0} \end{bmatrix}, \quad (22)$$

$$\begin{bmatrix} \boldsymbol{S}\left(\boldsymbol{a}, \alpha_{\mathrm{r}}\right) & -\boldsymbol{D}_{\mathrm{x}}^{\mathrm{T}} & -\boldsymbol{D}_{\mathrm{y}}^{\mathrm{T}} & 0 \\ l\boldsymbol{D}_{\mathrm{x}} & 0 & 0 & 0 \\ l\boldsymbol{D}_{\mathrm{y}} & 0 & 0 & 0 \\ l\boldsymbol{D}_{0} & 0 & 0 & -1 \end{bmatrix} \begin{bmatrix} \boldsymbol{a} \\ i_{\mathrm{x}} \\ i_{\mathrm{y}} \\ \psi_{0} \end{bmatrix} = \begin{bmatrix} \boldsymbol{f}_{\mathrm{pm}} + \boldsymbol{D}_{0}^{\mathrm{T}} i_{0} \\ \psi_{\mathrm{x}} \\ \psi_{\mathrm{y}} \\ 0 \end{bmatrix}, \quad (23)$$

in which $\boldsymbol{a}$ includes the nodal values of the magnetic vector potential, $\boldsymbol{S}(\boldsymbol{a},\alpha_{\mathrm{r}})$ is the magnetic stiffness matrix which depends on the solution and the rotor angle, $\boldsymbol{f}_{\mathrm{pm}}$ gives the source from the permanent magnets and l is the total axial length of the machine. Matrices $\boldsymbol{D}_{\mathrm{x}}$, $\boldsymbol{D}_{\mathrm{y}}$ and $\boldsymbol{D}_{0}$ describe the xy0 components of the flux linkage, and are obtained as

$$\begin{aligned} \boldsymbol{D}_{\mathrm{x}} &= \frac{2}{3}\sum_{k=1}^{3} \boldsymbol{D}_{k} \cos\left(\frac{2\pi}{3}(k-1)\right) \\ \boldsymbol{D}_{\mathrm{y}} &= \frac{2}{3}\sum_{k=1}^{3} \boldsymbol{D}_{k} \sin\left(\frac{2\pi}{3}(k-1)\right) \\ \boldsymbol{D}_{0} &= \frac{1}{3}\sum_{k=1}^{3} \boldsymbol{D}_{k} \end{aligned} \quad (24)$$

in which $\boldsymbol{D}_{k}$, k = 1, …, 3 give the flux linkages for the three phase windings, respectively.

Time-stepping FE simulations are used to verify the implemented state-space models. In the time-stepping FEM the system is supplied by the terminal voltages $\boldsymbol{v}$, and the phase currents are solved in the system together with the vector potential:

$$\begin{bmatrix} \boldsymbol{S}\left(\boldsymbol{a}, \alpha_{\mathrm{r}}\right) & -\left(\boldsymbol{KD}\right)^{\mathrm{T}} \\ \boldsymbol{0} & R_{\mathrm{s}}\boldsymbol{K}\boldsymbol{K}^{\mathrm{T}} \end{bmatrix} \begin{bmatrix} \boldsymbol{a} \\ \boldsymbol{i} \end{bmatrix} + \begin{bmatrix} \boldsymbol{T} & \boldsymbol{0} \\ l\boldsymbol{KD} & \boldsymbol{0} \end{bmatrix} \frac{d}{dt}\begin{bmatrix} \boldsymbol{a} \\ \boldsymbol{i} \end{bmatrix} = \begin{bmatrix} \boldsymbol{f}_{\mathrm{pm}} \\ \boldsymbol{Q}\boldsymbol{v} \end{bmatrix}, \quad (25)$$

in which $\boldsymbol{T}$ is the damping matrix related to eddy currents in conducting regions and $\boldsymbol{K}$ and $\boldsymbol{Q}$ are related to the connection of the stator winding (p. 39 of [11]). In star connection, only two independent currents $\boldsymbol{i} = \boldsymbol{i}_{\mathrm{ab}}$ are solved, $\boldsymbol{i}_{\mathrm{abc}} = \boldsymbol{K}\boldsymbol{i}_{\mathrm{ab}}$, and $\boldsymbol{v} = [v_{\mathrm{ab}}, v_{\mathrm{bc}}]^{\mathrm{T}}$. In case of delta connection, $\boldsymbol{i} = \boldsymbol{i}_{\mathrm{abc}}$, $\boldsymbol{v} = [v_{\mathrm{ab}}, v_{\mathrm{bc}}, v_{\mathrm{ca}}]^{\mathrm{T}}$, and $\boldsymbol{K}$ is an identity matrix. In the latter case, the zero-sequence current can flow freely. The torque is calculated from the FE solution with the Coulomb's method [26].

The static FE simulations for the identification of the flux-current relationships were performed for all required combinations of the four state variables $\boldsymbol{i}_{\mathrm{xy}}$ or $\boldsymbol{\psi}_{\mathrm{xy}}$, i_0 or ψ_0, and α_{r}. The rms and zero-sequence values of the current and flux were discretized in seven equally distributed values, while 60 values were used in the discretization of the space-vector and rotor angles (i.e. five steps per one stator slot pitch). For all combinations of the four state variables, this yielded 176400 static FE simulations in total for one model. Each one of the three sets of simulations for the CBM, FBM and HM took approximately 30 hours with the 2nd-order FE mesh of Fig. 1.

IV. Application and Results

A. Application

The test machine was simulated in several operation points in the motoring mode of operation with sinusoidal voltage supply. In Simulink, the simulations were done with the variable-step solver *ode45* with a maximum time-step size corresponding to 80 steps per one supply period. The FE model was simulated using the trapezoidal time-integration rule with fixed step size of 80 steps per one supply period.

In the state-space and time-stepping FE simulations the rotor angle was iterated so that the desired shaft powers were obtained. As a measure for the validity of the models, the power balance of the machine was calculated as

$$r_{\mathrm{p}} = \frac{P_{\mathrm{in}} - P_{\mathrm{out}} - P_{\mathrm{loss}}}{P_{\mathrm{in}}}, \quad (26)$$

in which P_{in} and P_{out} are the input and output powers, i.e., the

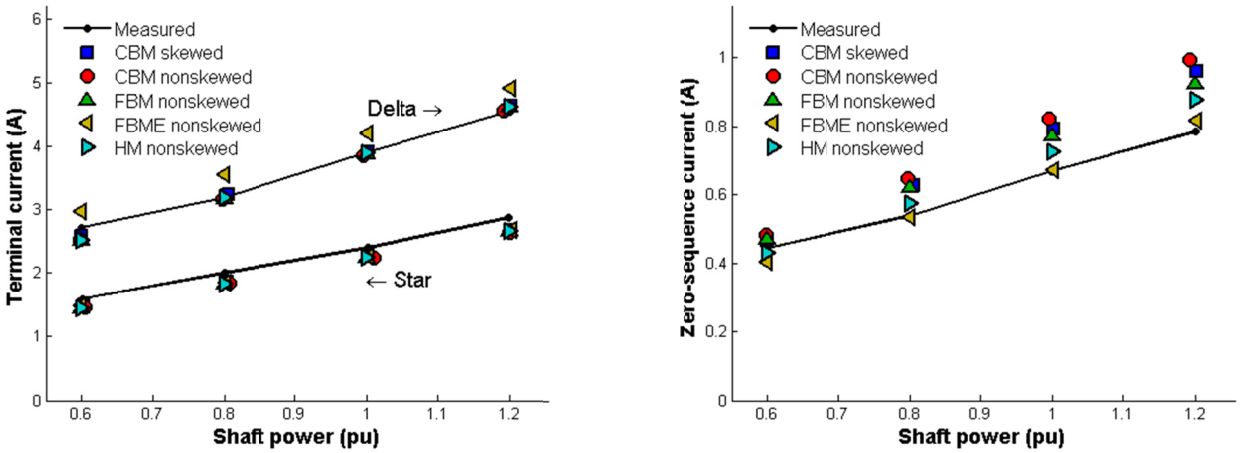

a) b)

Fig. 3 Measurement and simulation results on a) terminal currents in both star and delta connections and b) zero-sequence currents in delta connection.

active electrical and mechanical powers in the motoring mode of operation, respectively. P_{loss} includes the losses, meaning only the resistive losses in the state-space models but also the eddy-current losses in the permanent magnets and the shaft in the time-stepping FE model. However, these eddy-current losses are very small.

B. Comparison of Models and Measurements

We first verify the state-space models by comparison to measurements with the test machine. Fig. 3 a) shows the simulated and measured rms terminal currents in both star and delta connections with different loads while b) shows the rms zero-sequence currents in delta connection. A good correspondence is observed to the measurement results, which verifies the FE model and the state-space models derived from the static FE results. The FBME slightly exaggerates the terminal currents in delta connection, and the skewing is seen to slightly reduce the zero-sequence current at higher loads.

Fig. 4 compares the rated-load phase-current waveforms and spectrums in delta connection. All the models produce almost identical phase current waveforms, which correspond very well to the measured waveform. The effect of skewing can be seen to be negligible. In the spectrum, the third-harmonic component corresponds to the zero-sequence current.

The measured and simulated rated-load results and the simulation times are more carefully compared in Table II. All the state-space models predict the terminal currents and powers equally to the FE model in a fraction of computation time. Indeed, the non-skewed CBM, FBM and HM, respectively, are 350, 860 and 570 times faster than the FE model in the star connection and 350, 680 and 570 times faster in the delta connection. Modeling two slices in the CBM reduces the speed by 30 %. The FBME performs poorer than the other models because of the online differentiation of the energy but, as initially expected, satisfies the power balance better.

Opposite to the simulations, the measured terminal power is greater in star connection than in delta connection. This is most likely caused by the fact that the iron losses are smaller

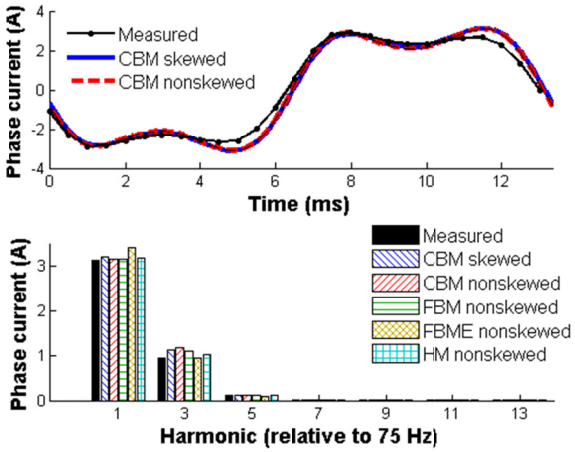

Fig. 4 Comparison of measured and simulated phase-current waveforms and spectrums in the rated operation point in delta connection.

in delta connection since the phase voltage is sinusoidal and the zero-sequence flux is smaller.

C. Zero-Sequence Effects

As is clearly visible in Table II, the machine has a much higher torque ripple in delta connection than in star connection. Fig. 5 compares the torque spectrums in both cases and shows that especially the sixth-harmonic torque component increases significantly in delta connection. Notable is that in case of this machine, the sixth harmonic is a much more severe problem than the cogging torque, which is seen as the 12th harmonic and is efficiently reduced by the skewing.

Using time-stepping FE analysis we demonstrate that the increase in the sixth-harmonic torque component is caused by the zero-sequence current. The machine is simulated in both star and delta connections with open stator terminals. In both cases the current space vector is zero, and thus the differences in the torque waveforms between the two cases are caused by the zero-sequence current which is present in delta connection but not in star. With open terminals, the zero-sequence flux arises only from the magnetic saturation, and thus we

TABLE II
RATED-LOAD RESULTS OF THE MEASUREMENTS, STATE-SPACE MODELS AND TIME-STEPPING FE MODEL IN BOTH STAR AND DELTA CONNECTIONS (WITH 80 TIME STEPS PER SUPPLY PERIOD AND TOTAL TIME OF 20 PERIODS IN THE SIMULATIONS)

Connection / Quantities / Simulation results		Skewed		Nonskewed				
		Measured	CBM	CBM	FBM	FBME	HM	FEM
Star connection	Number / type of lookup tables	-	12 (linear)	6 (linear)	3 (linear)	1 (cubic)	3 (linear)	-
	Terminal current (A)	2.40	2.23	2.22	2.23	2.22	2.23	2.22
	Zero-sequence current (A)	-	-	-	-	-	-	-
	Active power (kW)	2.57	2.35	2.34	2.37	2.36	2.37	2.35
	Power factor	0.96	0.95	0.96	0.96	0.96	0.96	0.95
	Displacement factor	-	0.948 ind	0.955 ind	0.958 ind	0.956 ind	0.958 ind	0.960 ind
	Torque (Nm)	14.0	14.0	14.0	14.0	14.0	14.0	14.0
	Torque THD (%)	-	1.20	1.63	1.38	1.40	1.38	1.60
	Resistive losses (W)	-	161	159	160	160	160	159
	Mechanical power (kW)	2.20	2.20	2.20	2.20	2.20	2.20	2.20
	Pole angle	-	35.3°	27.7°	28.0°	27.9°	28.0°	28.0°
	Power balance error	-	-0.59 %	-0.60 %	0.28 %	-0.08 %	0.23 %	-0.37 %
	Total simulation time (s)	-	0.50	0.39	0.21	1.42	0.31	177
	Time per time step (ms)	-	0.31	0.24	0.13	0.89	0.20	111
	Relative to real time	-	1.89	1.46	0.77	5.31	1.17	666
Delta connection	Number / type of lookup tables	-	20 (linear)	10 (linear)	4 (linear)	1 (cubic)	7 (linear)	-
	Terminal current (A)	3.89	3.89	3.87	3.88	4.08	3.89	3.86
	Zero-sequence current (A)	0.67	0.80	0.84	0.77	0.69	0.74	0.77
	Active power (kW)	2.41	2.36	2.36	2.39	2.39	2.39	2.37
	Power factor	0.96	0.89	0.89	0.91	0.88	0.91	0.91
	Displacement factor	-	0.947 ind	0.954 ind	0.961 ind	0.916 ind	0.962 ind	0.960 ind
	Torque (Nm)	14.0	14.0	14.0	14.0	14.0	14.0	14.0
	Torque THD (%)	-	4.28	4.91	4.41	5.34	4.58	4.78
	Resistive losses (W)	-	184	184	181	195	180	179
	Mechanical power (kW)	2.20	2.20	2.20	2.20	2.20	2.20	2.20
	Pole angle	-	35.2°	27.5°	27.3°	27.0°	27.4°	27.4°
	Power balance error	-	-0.99 %	-0.97 %	0.20 %	-0.09 %	0.42 %	-0.37 %
	Total simulation time (s)	-	0.50	0.39	0.26	6.54	0.31	177
	Time per time step (ms)	-	0.31	0.24	0.16	4.09	0.20	111
	Relative to real time	-	1.89	1.45	0.98	24.5	1.17	664

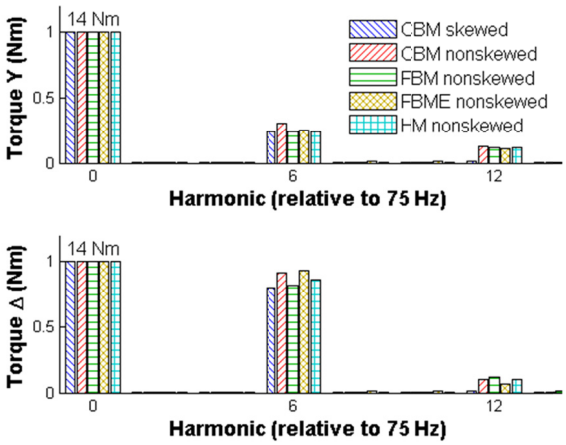

Fig. 5 Comparison of simulated torque spectrums in star (Y) and delta (Δ) connections.

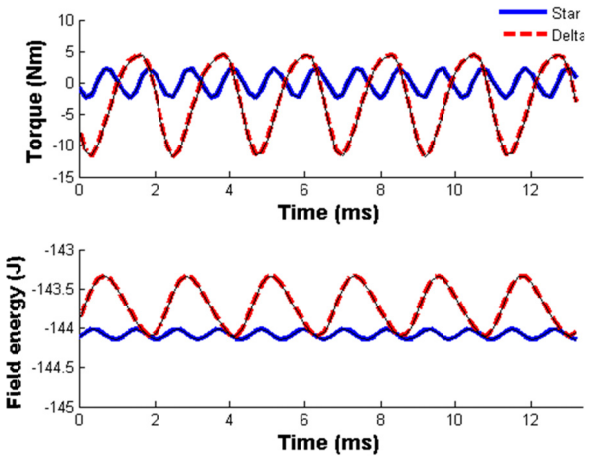

Fig. 6 FE-simulated torque and field energy in open-circuit operation in star and delta connections and exaggerated PM remanence.

exaggerate the saturation of the machine for this simulation by increasing the remanence flux density of the magnets up to 4 T in order to have clear differences between star and delta connections. The simulation results for both the instantaneous torque and field energy are shown in Fig. 6. Both the torque and energy have significant sixth-harmonic components in delta connection when the zero-sequence current flows in the windings. In the delta-connected case the average torque is negative since the resistive losses are supplied through the shaft.

In addition to the torque ripple, the zero-sequence current increases the losses of the machine. As seen from Table II, the modeled resistive losses are 12-22 % higher in delta connection than in star connection.

V. Discussion and Conclusions

After coupled with static FE simulation data, the implemented state-space models predict the currents and torques with the accuracy of a time-stepping FE model, but only in a fraction of computation time. This makes the coupled FE-state-space modeling an attractive alternative to FE analysis when mainly the terminal quantities and torque are of interest and long simulations or results in several operation points are desired. Possible applications for the discussed models include design and testing of control and estimation algorithms, as well as fast validation and identification of analytical machine models. The studied approaches are suitable for modeling of any kind of machines in which eddy currents do not play a significant role in the energy conversion process. These include DC machines, PM machines, synchronous and switched reluctance machines, as well as wound-rotor induction machines.

As expected, derivation of both the torque and currents from the magnetic field energy yielded a consistent model in which the power balance is very well satisfied. Although the energy-based model is somewhat slower than the models interpolating the quantities from look-up tables, it offers interesting possibilities from the implementation point-of-view, since no other variable than the field energy needs to be stored for the simulation. For example, a neural-network approach could be used to express the complicated dependency of the field energy on the state variables, which would allow analytical calculation of the required partial derivatives.

No major differences were observed in the results of the different models. The biggest advantage of the current-based approach is the possibility to couple several axial slices together in order to model skewing and other axial effects, which are discussed in more details in [21]. The flux-based approach requires fewer lookup tables than the current-based model, but requires using different FE results for the star and delta connections. The hybrid model suits well for both connections but prevents using the energy-based derivations.

The previously observed but not much discussed effect of the zero-sequence current on the torque ripple was demonstrated using FE analysis. In case of the studied machine, the zero-sequence also caused a significant increase in the losses in delta connection. These effects may need to be considered when electrically and thermally designing the machines described in [23], [24].

References

[1] T. M. Jahns, G. B. Kliman, T. W. Neumann, "Interior Permanent-Magnet Synchronous Motors for Adjustable Speed Drives," *IEEE Trans. Ind. Appl.*, Vol. IA-22, No. 4, pp. 738-747, July/August 1986.

[2] J. A. Guëmes, A. M. Iraolagoitia, J. I. Del Hoyo, P. Fernándezm "Torque Analysis in Permanent-Magnet Synchronous Motors: A Comparative Study," *IEEE Trans. Energy Convers.*, Vol. 26, No. 1, pp. 55-63, March 2011.

[3] A. K. Wallace, R. Spée, "The Effects of Motor Parameters on the Performance of Brushless DC Drives," *IEEE Trans. Power Electron.*, Vol. 5, No. 1, pp. 2-8, January 1990.

[4] T. S. Low, K. J. Tseng, T. H. Lee, K. W. Lim, K. S. Lock, "Strategy for the instantaneous torque control of permanent-magnet brushless DC drives," *IEE Proc. B. Electr. Power Appl.*, Vol. 137, No. 6, pp. 355-363, November 1990.

[5] F. Colamartino, C. Marchand, A. Razek, "Torque Ripple Minimization in Permanent Magnet Synchronous Servodrive," *IEEE Trans. Energy Convers.*, Vol. 14, No. 3, pp. 616-621, September 1999.

[6] V. Petrović, A. M. Stanković, "Modeling of PM Synchronous Motors for Control and Estimation Tasks," in *Proc. CDC*, 2001, pp. 2229-2234.

[7] K. A. Corzine, B. T. Kuhn, S. D. Sudhoff, H. J. Hegner, "An Improved Method for Incorporating Magnetic Saturation in the q-d Synchronous Machine Model," *IEEE Trans. Energy Convers.*, Vol. 13, No. 13, pp. 270-275, September 1998.

[8] S. Jurkovic, E. G. Strangas, "Design and Analysis of a High-Gain Observer for the Operation of SPM Machines Under Saturation," *IEEE Trans. Energy Convers*., Vol. 26, No. 2, pp. 417-427, June 2011.

[9] Z. Qu, T. Tuovinen, M. Hinkkanen, "Inclusion of Magnetic Saturation in Dynamic Models of Synchronous Reluctance Motors," in *Proc. ICEM*, 2012, pp. 994-1000.

[10] M. P. Krefta, O. Wasynczuk, "A Finite Element Based State Model of Solid Rotor Synchronous Machines," *IEEE Trans. Energy Convers.*, Vol. EC-2, No 1, pp. 21-30, March, 1987.

[11] A. Arkkio, "Analysis of Induction Motors Based on the Numerical Solution of the Magnetic Field and Circuit Equations," Ph.D. thesis, Helsinki University of Technology, Espoo, Finland, 1987. Available at http://lib.tkk.fi/Diss/198X/isbn951226076X/.

[12] O. A. Mohammed, S. Liu, Z. Liu, "Physical Modeling of PM Synchronous Motors for Integrated Coupling With Machine Drives," *IEEE Trans. Magn.*, Vol. 41, No. 5, pp. 1628-1631, May 2005.

[13] O. A. Mohammed, S. Liu, Z. Liu, "FE-based physical phase variable model of PM synchronous machines under stator winding short circuit faults," *IET Sci. Meas. Technol.*, Vol. 1, No. 1, pp. 12-16, January 2007.

[14] A. Sarikhani, O. A. Mohammad, "Sensorless Control of PM Synchronous Machines by Physics-Based EMF Observer," *IEEE Trans. Energy Convers.*, Vol. 27, No. 4, pp. 1009-1017, December 2012.

[15] S. Kallio, K. Karttunen, M. Adriollo, P. Peltoniemi, P. Silventoinen, "Finite Element Based Phase-Variable Model in the Analysis of Double-Star Permanent Magnet Machines," in *Proc. SPEEDAM*, 2012, pp. 1462-1467.

[16] S. Kallio, M. Andriollo, A. Tortella, J. Karttunen, "Decoupled *d-q* Model of Double-Star Interior-Permanent-Magnet Synchronous Machines," *IEEE Trans. Ind. Electron*., Vol. 60, No. 6, pp. 2486-2494, June 2013.

[17] C. Dufour, J. Bélanger, V. Lapointe, S. Abourida, "Real-Time Simulation on FPGA of a Permanent Magnet Synchronous Machine Drive Using a Finite-Element Based Model," in *Proc. SPEEDAM*, 2008, pp. 19-25.

[18] C. Dufour, H. Blanchette, J. Bélanger, "Very-high Speed Control of an FPGA-based Finite-Element-Analysis Permanent Magnet Synchronous MVirtual Motor Drive System," in *Proc. IECON*, 2008, pp. 2411-2416.

[19] M. Mohr, O. Biró, A. Stermecki, F. Diwoky, "An Improved Physical Phase Variable Model for Permanent Magnet Machines," in *Proc. ICEM*, 2012, pp. 53-58.

[20] M. Mohr, O. Biró, A. Stermecki, F. Diwoky, "Parameter Identification of a Finite Element Based Model of Wound Rotor Induction Machines," *COMPEL*, Vol. 32, No. 5, 2013.

[21] M. Mohr, O. Biró, A. Stermecki, F. Diwoky, "A Finite Element Based Circuit Model Approach for Skewed Electrical Machines," under review at *IEEE Trans. Magn.*, June 2013.

[22] R. J. Strahan, "Energy conversion by nonlinear permanent magnet machines," *IEE Proc. Electr. Power Appl.*, Vol. 145, No. 3, pp. 193-198, May 1998.

[23] M. V. Cistelecan, F. J. T. E. Ferreira, M. Popescu, "Adjustable Flux Three-Phase AC Machines With Combined Multiple-Step Star-Delta Winding Connections," *IEEE Trans. Energy Convers.*, Vol. 25, No. 2, pp. 348-355, June 2010.

[24] H. Vansompel, P. Sergeant, L. Dupré, A. Van den Bossche, "A Combined Wye-Delta Connection to Increase the Performance of Axial-Flux PM Machines With Concentrated Windings," *IEEE Trans. Energy Convers.*, Vol. 27, No. 2, pp. 403-410, June 2012.

[25] A. Arkkio, A. Hannukainen, "Proper finite-element discretization for torque computation of cage induction motors," in *Proc. SPEEDAM*, 2012, pp. 1456-1461.

[26] J. L. Coulomb, "A Methodology for the Determination of Global Electromechanical Quantities from a Finite Element Analysis and Its Application to the Evaluation of Magnetic Forces, Torques and Stiffness," *IEEE Trans. Magn.*, Vol. 19, No. 6, pp. 2514-2519, November 1983.

Paavo Rasilo was born in Äänekoski, Finland in 1983. He received his M.Sc. (Tech.) and D.Sc. (Tech.) degrees from Helsinki University of Technology (currently Aalto University) and Aalto University, Espoo, Finland in 2008 and 2012, respectively. He is currently visiting the Department of Electrical Energy, Systems and Automation at the Ghent University, Ghent, Belgium. His research interests deal with numerical modeling of electrical machines as well as power losses and magnetomechanical effects in soft magnetic materials.

Marc-Antoine Lemesle was born in Châteaubriant, France in 1991. He received his B.Sc. of electrical engineering from Nantes university school. He is currently pursuing his M.Sc. degree in the School of Electrical Engineering at Polytech Nantes in Saint Nazaire. In the 2nd year of his studies, he carries out an option: control of energies.

Anouar Belahcen was born in Essaouira, Morocco, in 1963. He received the B.Sc. degree in physics (Licence es-science) from the University Sidi Mohamed Ben Abdellah, Fes, Morocco, in 1988 and the M.Sc. (Tech.), LisTech, and Doctorate degrees from Helsinki University of Technology, Helsinki, Finland, in 1998, 2000, and 2004, respectively.

From 1996 to 1998, he was a Research Assistant at the Laboratory of Electromechanics, Helsinki University of Technology. From 1998 to 2004, he was a Research Scientist and from 2004 to 2008 he was a Senior Researcher at the same Laboratory. Since 2008, he has been working as an Adjunct Professor in the field of coupled problems and material modeling at the Department of Electrical Engineering, School of Electrical Engineering, Aalto University, Espoo, Finland. His research interests deal with the numerical modeling of electrical machines, especially magnetic material modeling, coupled magnetic and mechanical problems, magnetic forces, and magnetostriction.

Antero Arkkio was born in Vehkalahti, Finland in 1955. He received his M.Sc. (Tech.) and D.Sc. (Tech.) degrees from Helsinki University of Technology in 1980 and 1988. Currently he is a Professor of Electrical Engineering at Aalto University. His research interests deal with modeling, design, and measurement of electrical machines.

Marko Hinkkanen (M'06-SM'13) was born in Rautjärvi, Finland in 1975. He received his M.Sc. (Eng.) and D.Sc. (Tech.) degrees from Helsinki University of Technology, Espoo, Finland, in 2000 and 2004, respectively.

Since 2000, he has been with Helsinki University of Technology (part of Aalto University, Espoo, since 2010). He is currently an Assistant Professor with the Aalto University School of Electrical Engineering. His research interests include power-electronic converters, electric machines, and electric drives.